ARTICLE IN PRESS

Available online at www.sciencedirect.com

ScienceDirect

Comput. Methods Appl. Mech. Engrg. ▮ (▮▮▮▮) ▮▮▮–▮▮▮

Computer methods in applied mechanics and engineering

www.elsevier.com/locate/cma

An "immersed" finite element method based on a locally anisotropic remeshing for the incompressible Stokes problem

F. Auricchio[a,c], F. Brezzi[b,c], A. Lefieux[a,b,*], A. Reali[a,b,c]

[a] Dipartimento di Ingegneria Civile e Architettura (DICAr), Università degli Studi di Pavia, Via Ferrata 1, 27100, Pavia, Italy
[b] Centro di Simulazione Numerica Avanzata (CESNA-IUSS), Pavia, Italy
[c] Istituto di Matematica Applicata e Tecnologie Informatiche (IMATI-CNR), Pavia, Italy

Received 4 June 2014; received in revised form 30 September 2014; accepted 3 October 2014

Abstract

In the present paper we study a finite element method for the incompressible Stokes problem with a boundary immersed in the domain on which essential constraints are imposed. Such type of methods may be useful to tackle problems with complex geometries, interfaces such as multiphase flow and fluid–structure interaction. The method we study herein consists in locally refining elements crossed by the immersed boundary such that newly added elements, called subelements, fit the immersed boundary. In this sense, this approach is of a fitted type, but with an original mesh given *independently* of the location of the immersed boundary. We use such a subdivision technique to build a new finite element basis, which enables us to represent accurately the immersed boundary and to impose strongly Dirichlet boundary conditions on it. However, the subdivision process may imply the generation of anisotropic elements, which, for the incompressible Stokes problem, may result in the loss of inf–sup stability even for well-known stable element schemes. We therefore use a finite element approximation, which appears stable also on anisotropic elements. We perform numerical tests to check stability of the chosen finite elements. Several numerical experiments are finally presented to illustrate the capabilities of the method. The method is presented for two-dimensional problems.

Keywords: Immersed boundary; Anisotropic elements; Inf–sup condition; Incompressible Stokes problem

1. Introduction

One of the key ingredients of the success of the finite element method is its flexibility in the representation of the geometry on which the problem is defined. However, for several applications with highly complex geometries or very localized singularities (such as interfaces and cracks), generating a correct geometry representation is a difficult task.

In this paper we study an alternative approach, that consists in using a mesh which does not fit *a priori* the geometry, or the singularities, of the problem. For this reason, we refer to such class of approaches as *immersed boundary*

* Corresponding author at: Centro di Simulazione Numerica Avanzata (CESNA-IUSS), Pavia, Italy. Tel.: +39 0382985016.
E-mail addresses: ferdinando.auricchio@unipv.it (F. Auricchio), brezzi@imati.cnr.it (F. Brezzi), adrien.lefieux@unipv.it (A. Lefieux), alessandro.reali@unipv.it (A. Reali).

http://dx.doi.org/10.1016/j.cma.2014.10.001
0045-7825/

Please cite this article in press as: F. Auricchio, et al., An "immersed" finite element method based on a locally anisotropic remeshing for the incompressible Stokes problem, Comput. Methods Appl. Mech. Engrg. (2015), http://dx.doi.org/10.1016/j.cma.2014.10.001

methods. In the literature, these methods may be found under several names such as embedded, unfitted and fictitious domain.

Many immersed boundary methods do not take into account explicitly the existence of the boundary and, as a consequence, they experience loss of accuracy. A possible solution consists in enriching the finite element basis on the elements that are crossed by the immersed boundary, such that the irregularity of the solution is taken into account. An example of methods using local enrichments are the so-called *eXtended Finite Element Method* (XFEM) (see the work of [1] for a presentation of the XFEM in the context considered in the present article, or [2] for a general overview of the method).

First difficulty of the XFEM is that classical enriched functions might not be smooth inside an element, which leads to one of the major issues associated with such a methodology, i.e., a correct integration on elements that contain discontinuous functions. Nevertheless, the enriched functions are piecewisely smooth and, since the boundaries or the singularities are codimension 1 with respect to the geometry of the problem, we may construct "subelements" on which we can use standard quadrature rules. It follows that an important work is required to compute geometric structures to integrate.

Second difficulty is the imposition of essential constraints since the finite element basis may not be interpolatory on the immersed boundary. A possible solution consists in weakly enforcing constraints inside elements. However, such a strategy is not an easy solution (see for instance [3] and references therein).

In [4] an alternative approach is proposed. The method consists in reconstructing standard shape functions on the previously described subelements. Such an operation is an easy task with respect to the computational work required to obtain a geometric representation of the subelements. Their strategy is to use a stabilized low order finite element scheme such that newly added degrees of freedom, resulting from the reconstruction of the mesh, may be eliminated, with the advantage of a direct impact on the size of the system to solve. Drawbacks of the method are twofold. Firstly, only low order elements can be used such that there are no additional degrees of freedom and a stabilized finite element scheme is needed to ensure stability. Secondly, low order elements have a poor representation of the geometry and higher order elements may be preferred.

In the present paper, we propose an approach similar to the one proposed by [4], but with higher order elements, starting from the Hood–Taylor. This approach is also similar to Octree and Delaunay mesh generation with boundary recovery (see, e.g., [5] or [6] and references therein). In a similar framework as proposed here, in [7,8] higher order elements are used for a fluid dynamics problem. However, both of these works employ a "smoothing" procedure in order to ensure a "good" shape of the refined elements. In particular, in [8] a geometric parameter is introduced to enforce well shaped elements. However, here we prefer not to use a smoothing procedure such that there is no change in the distribution of the vertices of the original mesh. An important consequence of such a choice is that the subdivision process generates highly anisotropic elements. A possible effect of the distortion of the elements for the Stokes problem is a loss in the inf–sup stability, even for well known stable elements. In [9], it has been noted that the Hood–Taylor may lack of inf–sup stability on stretched meshes. They provide five numerical tests and the Hood–Taylor element fails three of them. They also showed that adding an extra bubble to the velocity field stabilizes the element for all tests provided. Since our application may generate different structures for the anisotropic elements, we propose a test inspired by the presented immersed approach to stress the stability of both finite element scheme by computing a Smallest Generalized Eigenvalue (SGE) test. We effectively show that P_2/P_1 may be unstable, whereas P_2^+/P_1 (i.e., P_2/P_1 with a cubic bubble on the velocity field) passes all SGE-tests. Additionally, we show with the SGE-test that the loss of stability of P_2/P_1 may occur within small triangles in corners for which both edges are constrained by a Dirichlet boundary condition. We then present more complex cases from real applications to check the results from the SGE-tests. We present a test for which no elements are constrained in a corner and we find that both schemes are stable. Hence, it appears that P_2/P_1 may be stable for a wide class of applications, but not for all, as we present two other problems where instability arises, as guessed from the SGE-test results. On the contrary, the inf–sup stability of P_2^+/P_1 element is always obtained.

The outline of the paper is as follows. In Section 2 we present the geometric aspects of the method, that is, the immersed boundary construction and the mesh representation. In Section 3 we first present the incompressible Stokes model and then a fundamental difficulty of a classical immersed method in imposing essential constraints; we then introduce the proposed method along with its subdivision process. In Section 4 we review the inf–sup condition and its implications in the case of anisotropic elements. We also present a numerical method to compute the inf–sup constants for the adopted finite element schemes, i.e., the SGE-test. In Section 5 we apply the SGE-test to three problems to

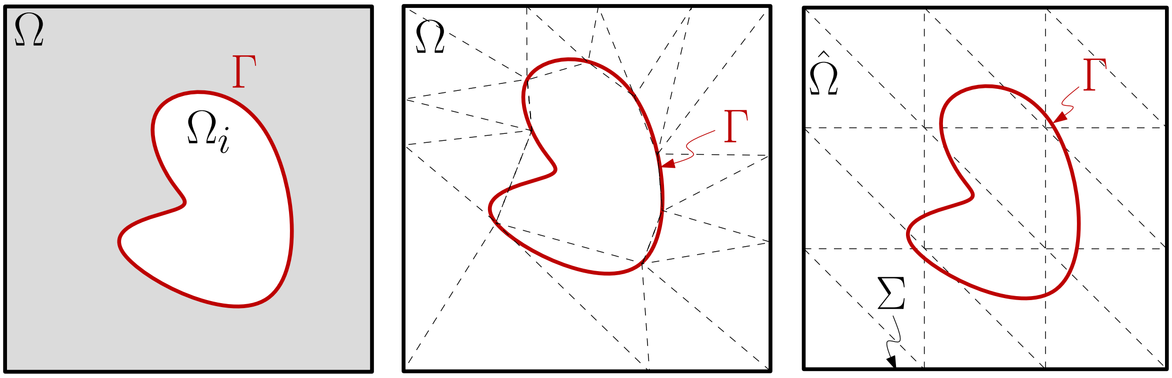

(a) Physical domain. (b) Fitted grid. (c) Unfitted grid.

Fig. 1. Fitted and unfitted discretizations of the physical region Ω : Ω_i is the interior (non physical) domain, Γ is the immersed boundary, $\Sigma = \partial\hat{\Omega}$ is the external boundary, and $\hat{\Omega} := \Omega \cup \Omega_i \cup \Gamma$ is the discretized domain.

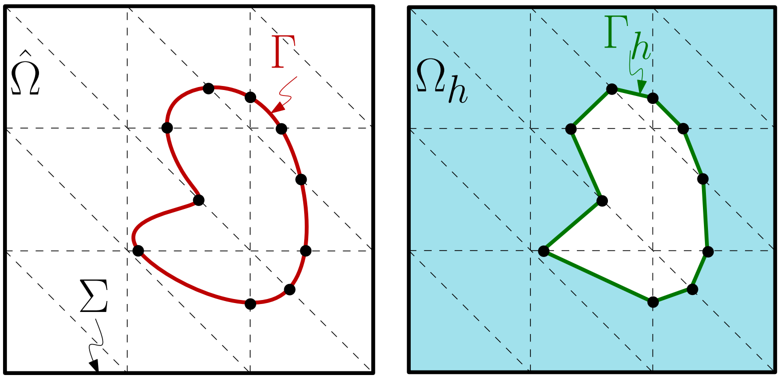

(a) Immersed boundary and a triangulation of $\hat{\Omega}$. (b) Interface reconstruction (in green) and integration domain (in blue).

Fig. 2. Description of the interface reconstruction process. The immersed boundary is denoted by Γ and the linear reconstruction of the immersed boundary, with respect to the background mesh, is denoted by Γ_h. In the remainder of the paper we also consider the integration domain Ω_h (in blue), defined such that $\partial\Omega_h = \Sigma \cup \Gamma_h$. (For interpretation of the references to color in this figure legend, the reader is referred to the web version of this article.)

assess the stability of the P_2/P_1 and P_2^+/P_1 elements, and we test the method on three real flow problems. Finally, we draw our conclusions in Section 6.

2. Geometry

In this section we consider the geometric aspects of the method, i.e., the problem of the construction of a mesh conveniently discretizing the considered physical domain. Two strategies are possible: "fitted" or "unfitted" (cf. Fig. 1).

In the fitted approach the discretized domain fits the boundary of the problem, while in the unfitted approach the physical domain is a subset of the discretization. More precisely, in the unfitted case, we consider a problem defined on $\Omega \subset \mathbb{R}^2$ such that a part of the boundary of $\partial\Omega$, denoted by Γ (named *immersed boundary*), is not fitted *a priori* by the triangulation of $\hat{\Omega}$, with $\Omega \subset \hat{\Omega}$. The part of the boundary $\partial\Omega$ that is fitted by the triangulation of $\hat{\Omega}$ is denoted by Σ.

We illustrate the problem in Fig. 1(c). To avoid the difficulties and the costs connected with the generation of fitted meshes in complicated situations, we propose to start with a regular unfitted mesh $\hat{\Omega}$ and to represent Γ by a linear reconstruction on such a triangulation, as illustrated in Fig. 2. The reconstruction procedure is presented in detail in the next section.

Please cite this article in press as: F. Auricchio, et al., An "immersed" finite element method based on a locally anisotropic remeshing for the incompressible Stokes problem, Comput. Methods Appl. Mech. Engrg. (2015), http://dx.doi.org/10.1016/j.cma.2014.10.001

2.1. Interface reconstruction

We assume that a regular triangulation $\hat{\mathcal{T}}$ of $\hat{\Omega}$ (named *background* mesh) and the interface Γ satisfy the conditions presented in [10], that is the boundary Γ crosses once two triangle edges. We note that there always exists a sufficiently fine triangulation of $\hat{\Omega}$ such that the conditions are fulfilled for any smooth immersed boundary. The reconstructed boundary of Γ is denoted Γ_h and it is the linear interpolation of all intersections with the background mesh edges. It follows that the reconstructed interface is a segment in each intersected element, and it defines a new domain Ω_h such that $\partial\Omega_h = \Sigma \cup \Gamma_h$ (cf. Fig. 2). Domain Ω_h is referred to as integration domain. We point out that the linear reconstruction of Γ is not a limitation of the method we propose and that, in a case with a curved immersed boundary, isoparametric elements may be used, as well as more complex algorithms, to describe the boundary.

We consider such types of methods as belonging to an "intersection class" of methods, since they require to compute intersection points between the immersed boundary and the mesh. On the contrary, for instance, the Finite Cell Method (see [11]) or the approach recently proposed in [12] does not belong to this class of methods. Knowing intersection points allows a subdivision of the mesh, which may be used for integration, construction of shape functions, etc. We point out that computing the intersection points is very demanding in terms of computational cost, and it is a fundamental part of all codes using such an approach.

3. Model problem: Incompressible Stokes

Let $\Sigma = \Sigma_D \cup \Sigma_N$ where Σ_D denotes the part of the external boundary on which we impose a Dirichlet boundary condition and Σ_N the part on which we impose a Neumann boundary condition, whose value is assumed to be zero without loss of generality. On the other hand, we consider homogeneous Dirichlet boundary conditions on Γ but non homogeneous Dirichlet boundary conditions can be applied as well. Neumann boundary conditions are not considered here because they can be enforced "naturally" in the variational formulation, and as a consequence, they are easier to tackle. The model problem we consider in this paper is given by the following standard weak form of the incompressible Stokes equation:

Problem 1. Find $(\mathbf{u}, p) \in \boldsymbol{V}(\Omega) \times Q(\Omega)$ such that $\forall(\mathbf{v}, q) \in \boldsymbol{V}_0(\Omega) \times Q(\Omega)$:

$$\begin{cases} \displaystyle\int_\Omega \nabla\mathbf{u} : \nabla\mathbf{v}\, d\Omega - \int_\Omega p\, \mathrm{div}(\mathbf{v})\, d\Omega = \int_\Omega \mathbf{f}\cdot\mathbf{v}\, d\Omega, \\ \displaystyle\int_\Omega q\, \mathrm{div}(\mathbf{u})\, d\Omega = 0, \end{cases} \tag{1}$$

where

$$\begin{cases} \boldsymbol{V}(\Omega) := \{\mathbf{v} \in [H^1(\Omega)]^2;\ \mathbf{v}_{|\Sigma_D} = \mathbf{u}_D \text{ and } \mathbf{v}_{|\Gamma} = \mathbf{0}\}, \\ \boldsymbol{V}_0(\Omega) := \{\mathbf{v} \in [H^1(\Omega)]^2;\ \mathbf{v}_{|\Sigma_D} = \mathbf{0} \text{ and } \mathbf{v}_{|\Gamma} = \mathbf{0}\}, \\ Q(\Omega) := L^2(\Omega). \end{cases}$$

Remark 1. The constraint $\mathbf{u}_{|\Gamma} = \mathbf{0}$ is strongly enforced since it is imposed in the trial and test spaces. On the contrary, the incompressibility constraint is enforced weakly in the formulation and the pressure p is the corresponding Lagrange multiplier. We note, that since a weak imposition of a constraint with a Lagrange multiplier results in a saddle point problem, we have to choose a stable pair of elements for the velocity and the pressure satisfying an inf–sup condition (see, e.g., [13]). This issue is discussed further in Section 4. We note that in the case Σ_N is empty then $Q(\Omega) := L^2(\Omega)/\mathbb{R}$.

3.1. A fundamental problem of unfitted methods

In this section we present a classical unfitted method (see the example in [14]) which consists in using the triangulation $\hat{\mathcal{T}}$ to build the finite element spaces and we point out its difficulties. We present the discretized problem with classical Hood–Taylor P_2/P_1 finite elements (but the method may be generalized). The considered problem reads:

Please cite this article in press as: F. Auricchio, et al., An "immersed" finite element method based on a locally anisotropic remeshing for the incompressible Stokes problem, Comput. Methods Appl. Mech. Engrg. (2015), http://dx.doi.org/10.1016/j.cma.2014.10.001

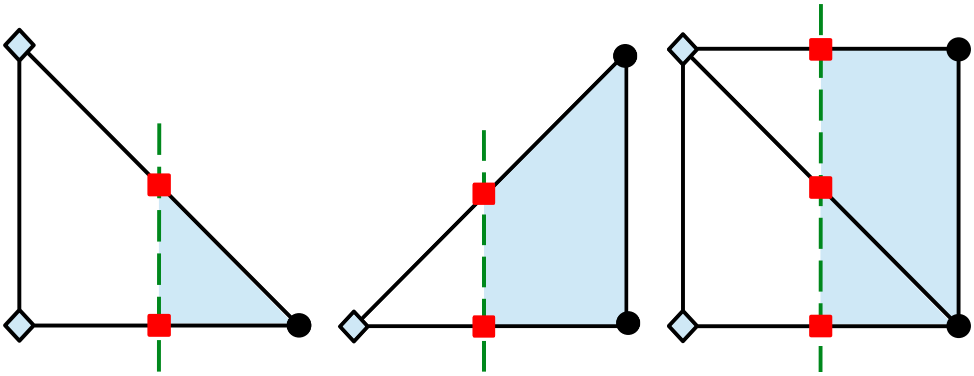

(a) Two internal constraints are satisfied since two "free" nodes are associated with it.

(b) The problem is overconstrained since only one "free" node is associated with the two internal constraints.

(c) This generic macro-element shows that the internal constraints cannot be imposed and thus locking occurs.

Fig. 3. In this example we consider a single field problem. The elements are P_1 and the physical domain is depicted in blue. It follows that the diamonds are "free" nodes (i.e., their values have no physical relevance) while the dots are physical nodes. We want to illustrate the difficulty of imposing the internal constraint $\mathbf{u} = \mathbf{0}$ on the red squares. (For interpretation of the references to color in this figure legend, the reader is referred to the web version of this article.)

Problem 2. Find $(\mathbf{u}_h, p_h) \in \boldsymbol{V}^h \times Q^h$ such that $\forall(\mathbf{v}_h, q_h) \in \boldsymbol{V}_0^h \times Q^h$:

$$\begin{cases} \displaystyle\int_{\Omega_h} \nabla\mathbf{u}_h : \nabla\mathbf{v}_h \, d\Omega_h - \int_{\Omega_h} p_h \operatorname{div}(\mathbf{v}_h) \, d\Omega_h = \int_{\Omega_h} \mathbf{f} \cdot \mathbf{v}_h \, d\Omega_h, \\ \displaystyle\int_{\Omega_h} q_h \operatorname{div}(\mathbf{u}_h) \, d\Omega_h = 0, \end{cases} \tag{2}$$

where

$$\begin{cases} \mathbf{V}^h := \{\mathbf{v} \in C^0(\hat{\Omega}); \mathbf{v}_{|T} \in [\mathcal{P}_2]^2, \mathbf{v}_{|\Sigma_D^h} = \mathbf{u}_D \text{ and } \mathbf{v}_{|\Gamma^h} = \mathbf{0}, \forall T \in \hat{\mathcal{T}}\} \subset \mathbf{V}(\hat{\Omega}), \\ \mathbf{V}_0^h := \{\mathbf{v} \in C^0(\hat{\Omega}); \mathbf{v}_{|T} \in [\mathcal{P}_2]^2, \mathbf{v}_{|\Sigma_D^h} = \mathbf{0} \text{ and } \mathbf{v}_{|\Gamma^h} = \mathbf{0}, \ \forall T \in \hat{\mathcal{T}}\} \subset \mathbf{V}_0(\hat{\Omega}), \\ Q^h := \{q \in C^0(\hat{\Omega}); q_{|T} \in [\mathcal{P}_1], \ \forall T \in \hat{\mathcal{T}}\} \subset L^2(\hat{\Omega}), \end{cases}$$

where $\hat{\mathcal{T}}$ is a triangulation of $\hat{\Omega}$, $\mathcal{P}_k$ is the space of polynomials of degree k, and Σ_D^h is the discrete external Dirichlet boundary.

It is important to note that in Problem 2 the integration is performed on Ω_h and not on $\hat{\Omega}$ (see Section 3.2.1 for a subdivision strategy of $\hat{\Omega}$ to perform the quadrature). Indeed, as discussed in [15] one cannot hope to obtain an optimal rate of convergence if the integration is performed on $\hat{\Omega}$. This result is independent of how the constraint $\mathbf{u} = \mathbf{0}$ on Γ is imposed.

For the considered problem, it is not possible to obtain the optimal rate of convergence because the spaces $\boldsymbol{V}^h$ and $\boldsymbol{V}_0^h$ are not rich enough (see [14] for more details). We illustrate this issue in Fig. 3. Indeed, for a general set of elements there are more constraints on the immersed boundary (i.e., at the intersection of the immersed boundary with the background mesh element edges) than nodes of the intersected elements that do not belong to the physical domain (named "free nodes"). As a consequence, the system is overconstrained and locking may occur. For example, in [16] an algorithm is presented such that two degrees of freedom are uniquely associated with an interface constraint. But, one of the drawbacks of the approach is that it weakens the imposition of the Dirichlet boundary constraint on the immersed boundary.

We point out that since it is not possible to strongly impose the condition $\mathbf{u} = \mathbf{0}$ on Γ_h in order to obtain the optimal rate of convergence, weak imposition of the Dirichlet condition is often used. A weak imposition can be performed, for instance, with a Lagrange multiplier (but checking the inf–sup condition for such a method is not an easy task, see [16] and references therein) or the Nitsche method which requires additional user parameters. Weak imposition of essential boundary conditions is still an active area of research (see for instance [17] for an example of the Nitsche

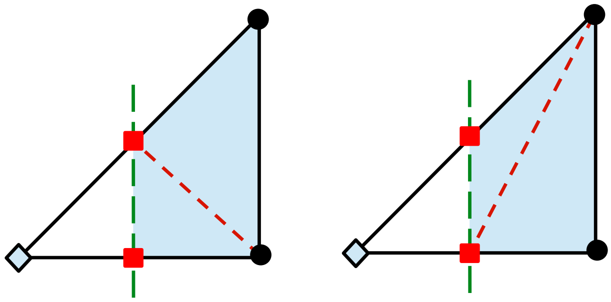

(a) Non unicity of the quadrilateral subdivision. The pair of triangles giving the smallest element ratios is selected (i.e., the pair on the left in this example).

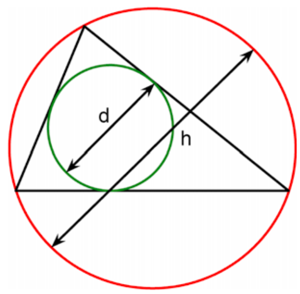

(b) The diameters of the circumscribed and inscribed circles are denoted h and d, respectively.

Fig. 4. Selection of the quadrilateral subdivision in subtriangles and description of the element ratio.

method for the Stokes problem or alternative approaches in [18] and [19]). The method we propose in the following avoids the use of complex strategies for weakly imposing essential boundary conditions. It consists in building a finite element basis that is interpolatory on the intersection points of the immersed boundary and the background mesh edges in order to impose Dirichlet boundary conditions strongly.

3.2. A method by a locally anisotropic remeshing

In the following, we propose a method that considers a special local remeshing using a subdivision of elements cut by the immersed boundary. The method differs from the classical one presented in Problem 2, which uses the triangulation $\hat{\mathcal{T}}$ to build the finite elements. The proposed method consists in refining all elements cut by the immersed boundary such that a locally fitting mesh may be built. In particular, we show that such a subdivision process may not lead to a unique subdivision into triangles and we present a strategy to select the best subdivision.

3.2.1. Subdivision

For triangles cut by the immersed boundary we consider the two cases, depending on if the subelement belonging to Ω_h is: (a) a triangle, or (b) a quadrilateral.

In the present work we consider finite elements only on triangles and thus in case (b) we have to subdivide the quadrilateral into two triangles. As depicted in Fig. 4(a), the subdivision into triangles of a quadrilateral is not unique, and therefore we propose a strategy to choose the best subdivision. The selection method for the subdivision of the quadrilateral into triangles is based on selecting the best element ratio pair, with the element ratio defined by

$$\sigma = \frac{h}{d},$$

where h and d are the diameters of the circumscribed and inscribed circles, respectively (see Fig. 4(b)).

Remark 2. It is clear that the subdivision may imply anisotropic elements. In two famous independent papers, ([20,21]) the *minimum angle condition* for triangles is introduced. The condition requires that the smallest angle of a triangle has to be bounded from below by a strictly positive real. The minimum angle condition is a sufficient (but not necessary) condition to guarantee the convergence of the finite element method. In [22,23] the *maximum angle condition* is introduced, which stipulates that the largest angle of a triangle has to be bounded above by a real strictly lower than π. Again the condition is sufficient to guarantee the optimal convergence of the finite element method. However, it has been noted in [24] that the maximum angle condition is not necessary and the finite element method for 2D problems may converge optimally without a maximum angle condition satisfied. Moreover, since we consider a saddle point problem, an inf–sup condition has to be satisfied as well, and finite element schemes that are stable on well shaped elements may not be stable on anisotropic ones. We discuss further this issue in Section 4.

Accordingly, in the following sections, we consider a triangulation $\mathcal{T}_r$ built as follows. Given a shape regular triangulation $\hat{\mathcal{T}}$ of $\hat{\Omega}$ (i.e., the background mesh), we denote by $\mathcal{T}_\Gamma$ the triangulation of all elements that are crossed by Γ. As previously explained it is possible to build a subtriangulation $\mathcal{T}_\Gamma'|_T$ on every $T \in \mathcal{T}_\Gamma$ such that $\mathcal{T}_\Gamma'$ fits Γ,

Please cite this article in press as: F. Auricchio, et al., An "immersed" finite element method based on a locally anisotropic remeshing for the incompressible Stokes problem, Comput. Methods Appl. Mech. Engrg. (2015), http://dx.doi.org/10.1016/j.cma.2014.10.001

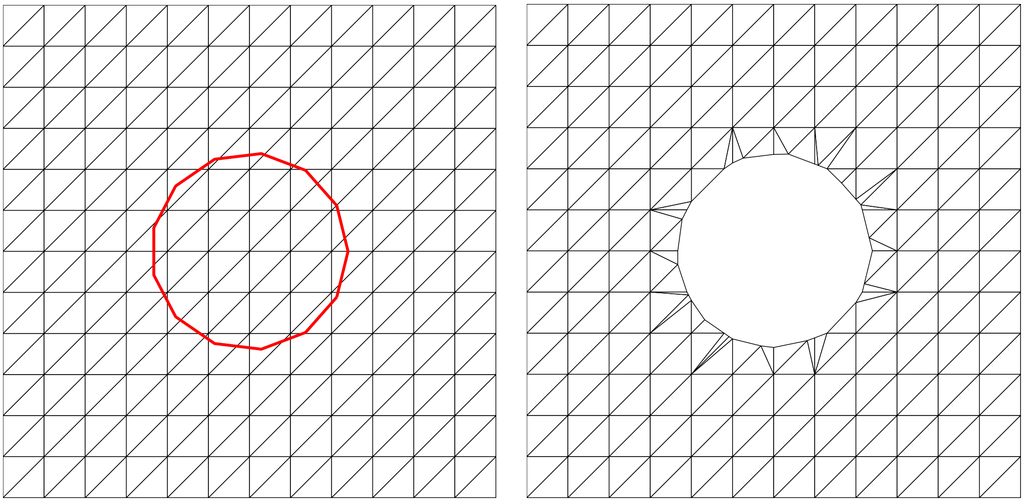

(a) Original mesh $\hat{\mathcal{T}}$.

(b) Refined mesh $\mathcal{T}_r$.

Fig. 5. Subdivision operation of $\hat{\mathcal{T}}$ into $\mathcal{T}_r$.

with respect to the linear reconstruction of Γ. Then, we consider the triangulation $\mathcal{T}_r$ made of all elements in $\hat{\mathcal{T}}$ that are entirely in Ω_h and all elements of $\mathcal{T}'_\Gamma$ that are in Ω_h. The operation is illustrated in Fig. 5 for the case of an immersed disk.

3.2.2. Application to the incompressible Stokes problem

In the following we give an example of the discretized Stokes problem using the locally anisotropic remeshing with the P_2/P_1 finite element scheme:

Problem 3. Find $(\mathbf{u}_h, p_h) \in \boldsymbol{W}^h \times R^h$ such that $\forall(\mathbf{v}_h, q_h) \in \mathbf{W}_0^h \times R^h$:

$$\begin{cases} \displaystyle\int_{\Omega_h} \nabla \mathbf{u}_h : \nabla \mathbf{v}_h \, \mathrm{d}\Omega_h - \int_{\Omega_h} p_h \operatorname{div}(\mathbf{v}_h) \, \mathrm{d}\Omega_h = \int_{\Omega_h} \mathbf{f} \cdot \mathbf{v}_h \, \mathrm{d}\Omega_h, \\ \displaystyle\int_{\Omega_h} q_h \operatorname{div}(\mathbf{u}_h) \, \mathrm{d}\Omega_h = 0, \end{cases} \tag{3}$$

where

$$\begin{cases} \mathbf{W}^h := \{\mathbf{v} \in C^0(\Omega_h); \mathbf{v}_{|T} \in [\mathcal{P}_2]^2, \mathbf{v}_{|\Sigma_D^h} = \mathbf{u}_D \text{ and } \mathbf{v}_{|\Gamma^h} = \mathbf{0}, \quad \forall T \in \mathcal{T}_r\} \subset \mathbf{V}(\Omega_h), \\ \mathbf{W}_0^h := \{\mathbf{v} \in C^0(\Omega_h); \mathbf{v}_{|T} \in [\mathcal{P}_2]^2, \mathbf{v}_{|\Sigma_D^h} = \mathbf{0} \text{ and } \mathbf{v}_{|\Gamma^h} = \mathbf{0}, \quad \forall T \in \mathcal{T}_r\} \subset \mathbf{V}_0(\Omega_h), \\ R^h := \{q \in C^0(\Omega_h); q_{|T} \in [\mathcal{P}_1], \quad \forall T \in \mathcal{T}_r\} \subset L^2(\Omega_h). \end{cases}$$

As we shall see later, such a scheme might not be a good choice for our method due to the instability of the Hood–Taylor element on anisotropic meshes. Therefore, we also consider the so-called P_2^+/P_1 element, whose finite element space, for our application, is defined by

$$\mathbf{W}^h := \{\mathbf{v} \in C^0(\Omega_h); \mathbf{v}_{|T} \in [\mathcal{P}_2 \oplus B_3]^2, \mathbf{v}_{|\Sigma_D^h} = \mathbf{u}_D \text{ and } \mathbf{v}_{|\Gamma^h} = \mathbf{0}, \ \forall T \in \mathcal{T}_r\}, \tag{4}$$

$$\mathbf{W}_0^h := \{\mathbf{v} \in C^0(\Omega_h); \mathbf{v}_{|T} \in [\mathcal{P}_2 \oplus B_3]^2, \mathbf{v}_{|\Sigma_D^h} = \mathbf{0} \text{ and } \mathbf{v}_{|\Gamma^h} = \mathbf{0}, \ \forall T \in \mathcal{T}_r\}, \tag{5}$$

where B_3 denotes the space of cubic bubble functions (see, e.g., [13] for more details).

Remark 3. As presented in Eq. (4) the bubbles are used on all elements of the mesh $\mathcal{T}_r$. In practice, we add the bubble only on subtriangles.

In Fig. 6 we compare the methods presented with Problem 2 and Problem 3. We note that the present method has more degrees of freedom than the original described method. In [4], which is based on a stabilized P_1/P_0 scheme, added

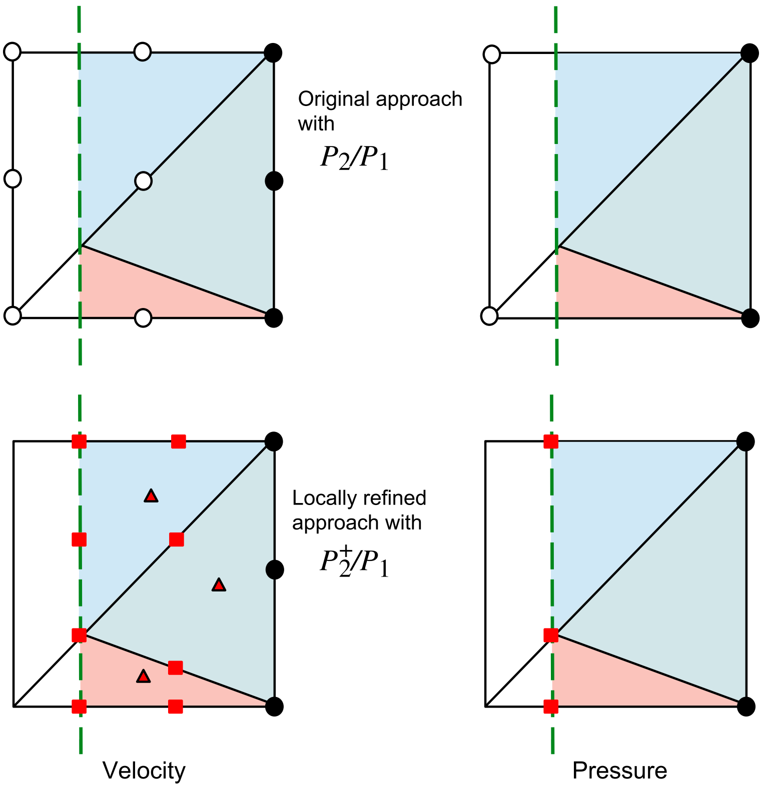

Fig. 6. Comparison between original P_2/P_1 (Problem 2) and locally refined P_2^+/P_1 (Problem 3). The black dots are common degrees of freedom in both approaches, white dots are eliminated degrees of freedom (i.e., the nodes that are present in the original method which are not present in the locally refined method), red squares are added degrees of freedom, and triangles are bubble degrees of freedom. (For interpretation of the references to color in this figure legend, the reader is referred to the web version of this article.)

discontinuous pressure degrees of freedom are eliminated by static condensation, while the new velocity degrees of freedom are actually Dirichlet boundary nodes.

4. The inf–sup condition on anisotropic elements

Given the approximations $\mathbf{u}_h = \sum_{i=1}^{n} \mathbf{N}_i \hat{\mathbf{u}}_i$ and $p_h = \sum_{i=1}^{m} M_i \hat{p}_i$, where $\mathbf{N}_i$ and M_i are the finite element bases for $\mathbf{W}^h$ and R^h (with n and m the number of degrees of freedom for the velocity and pressure fields, respectively) the discrete incompressible Stokes problem in matrix form reads

$$\begin{bmatrix} \mathbf{A} & \mathbf{B}^T \\ \mathbf{B} & \mathbf{0} \end{bmatrix} \begin{Bmatrix} \hat{\mathbf{u}} \\ \hat{\mathbf{p}} \end{Bmatrix} = \begin{Bmatrix} \hat{\mathbf{f}} \\ \hat{\mathbf{g}} \end{Bmatrix}, \tag{6}$$

where

$$\begin{cases} \mathbf{A}|_{ij} = \displaystyle\int_{\Omega_h} \nabla \mathbf{N}_i : \nabla \mathbf{N}_j \, \mathrm{d}\Omega_h & \forall (i, j) \in \{1, 2, \ldots, n\} \times \{1, 2, \ldots, n\}, \\ \mathbf{B}|_{ij} = -\displaystyle\int_{\Omega_h} M_i \operatorname{div}(\mathbf{N}_j) \, \mathrm{d}\Omega_h & \forall (i, j) \in \{1, 2, \ldots, m\} \times \{1, 2, \ldots, n\}. \end{cases}$$

Let $n+1, \ldots, n+n_D$ be the eliminated degrees of freedom lying on Σ_D, the right hand side reads

$$\begin{cases} \hat{\mathbf{f}}|_i = \displaystyle\int_{\Omega_h} \mathbf{f}_h \cdot \mathbf{N}_i \, \mathrm{d}\Omega_h - (\bar{\mathbf{A}} \hat{\mathbf{u}}_D)|_i & \forall i \in \{1, 2, \ldots, n\}, \\ \hat{\mathbf{g}}|_i = -(\bar{\mathbf{B}} \hat{\mathbf{u}}_D)|_i & \forall i \in \{1, 2, \ldots, m\}, \end{cases}$$

where

$$\begin{cases} \bar{\mathbf{A}}|_{ij} = \int_{\Omega_h} \nabla \mathbf{N}_i : \nabla \mathbf{N}_j \, \mathrm{d}\Omega_h & \forall (i,j) \in \{1,2,\ldots,n\} \times \{n+1, n+2, \ldots, n+n_D\}, \\ \bar{\mathbf{B}}|_{ij} = -\int_{\Omega_h} M_i \, \mathrm{div}(\mathbf{N}_j) \, \mathrm{d}\Omega_h & \forall (i,j) \in \{1,2,\ldots,m\} \times \{n+1, n+2, \ldots, n+n_D\}, \end{cases}$$

and $\hat{\mathbf{u}}_D$ are the nodal boundary values of $\mathbf{u}_D$.

In the following we also use the pressure mass matrix defined by

$$\mathbf{M}_{|ij} = \int_{\Omega_h} M_i M_j \mathrm{d}\Omega_h \quad \forall (i,j) \in \{1,2,\ldots,m\} \times \{1,2,\ldots,m\}. \tag{7}$$

The euclidean norm is given by $\|\hat{\mathbf{v}}\|_0^2 = \hat{\mathbf{v}}^T \hat{\mathbf{v}}$ with $\hat{\mathbf{v}} \in \mathbb{R}^n$. We also consider the norm defined by the stiffness matrix $\mathbf{A}$, that is $\|\hat{\mathbf{v}}\|_A^2 = \hat{\mathbf{v}}^T \mathbf{A}^T \hat{\mathbf{v}}$ and its associated dual norm given by $\|\hat{\mathbf{v}}\|_{A'}^2 = \hat{\mathbf{v}}^T \mathbf{A}^{-T} \hat{\mathbf{v}}$. Let $\hat{\mathbf{q}} \in \mathbb{R}^m$, then the norm used for the pressure field is given by $\|\hat{\mathbf{q}}\|_M^2 = \hat{\mathbf{q}}^T \mathbf{M}^T \hat{\mathbf{q}}$ and its associated dual norm by $\|\hat{\mathbf{q}}\|_{M'}^2 = \hat{\mathbf{q}}^T \mathbf{M}^{-T} \hat{\mathbf{q}}$, where $\mathbf{M}$ is defined in Eq. (7).

It is well known that a key component for Eq. (6) to have a unique solution is the satisfaction of the following condition (see, e.g., [13]):

Inf–sup: $\exists \beta_h > 0$ (independent of h) such that

$$\max_{\hat{\mathbf{v}} \in \mathbb{R}^n \setminus \{\mathbf{0}\}} \frac{\hat{\mathbf{v}}^T \mathbf{B}^T \hat{\mathbf{q}}}{|| \; \hat{\mathbf{v}} \; | \;|_A} \geq \beta_h \; || \; \hat{\mathbf{q}} \; | \;|_M \qquad \forall \hat{\mathbf{q}} \in \mathbb{R}^m. \tag{8}$$

Being $\hat{\mathbf{u}}^I$ and $\hat{\mathbf{p}}^I$ the vectors of analytical solutions at the nodes for the velocity and the pressure, respectively, an error estimate is given by (see, e.g., [13]):

$$\|\hat{\mathbf{u}}^I - \hat{\mathbf{u}}\|_A \leq C \left(\|\hat{\mathbf{f}}\|_{A'} + \beta_h^{-1} \|\hat{\mathbf{g}}\|_{M'} \right), \tag{9}$$

$$\|\hat{\mathbf{p}}^I - \hat{\mathbf{p}}\|_M \leq C \left(\beta_h^{-1} \|\hat{\mathbf{f}}\|_{A'} + \beta_h^{-2} \|\hat{\mathbf{g}}\|_{M'} \right), \tag{10}$$

where C denotes a general constant independent of h and β_h.

We clearly can see from Eqs. (9) and (10) that if $\beta_h \to 0$ as $\sigma \to \infty$ then the error for the pressure may not be bounded and it depends on $1/\beta_h^2$, while the velocity field may also not be bounded but it depends only on $1/\beta_h$.

We equip the space $\mathbf{V}$ and Q (see Eqs. (1)) with the norms

$$\begin{cases} \|\mathbf{v}\|_V^2 = \int_\Omega \nabla \mathbf{v} : \nabla \mathbf{v} \mathrm{d}\Omega, \\ \|q\|_Q^2 = \int_\Omega q^2 \mathrm{d}\Omega, \end{cases}$$

where $\mathbf{v} \in \mathbf{V}(\Omega)$ and $q \in Q(\Omega)$. Given that $\mathbf{u}^I = \sum_i \hat{\mathbf{u}}_i^I \mathbf{N}_i$ and $q^I = \sum_i \hat{q}_i^I M_i$ are the interpolant of the analytical solution using the finite element basis, it can be shown that (see [25])

$$\|\hat{\mathbf{u}}^I - \hat{\mathbf{u}}\|_A \leq C \left(\beta_h^{-1} \|\mathbf{u}^I - \mathbf{u}_h\|_V + \|p^I - p_h\|_Q \right), \tag{11}$$

$$\|\hat{\mathbf{p}}^I - \hat{\mathbf{p}}\|_M \leq C \left(\beta_h^{-2} \|\mathbf{u}^I - \mathbf{u}_h\|_V + \beta_h^{-1} \|p^I - p_h\|_Q \right). \tag{12}$$

To conclude, it is very important that for the chosen finite element β_h remains bounded from below as σ increases. In other words, we would like β_h to be independent of σ.

4.1. Numerical methods to measure the inf–sup condition (the Smallest Generalized Eigenvalue test)

In order to test if our finite element scheme of choice remains stable as σ increases, we compute numerically the inf–sup constant.

It can be proven that (see, e.g., [26]) the inf–sup constant β_h is given by the square root of the lowest positive eigenvalue of the following generalized eigensystem:

$$\mathbf{B}\mathbf{A}^{-1}\mathbf{B}^T\mathbf{q} = \lambda\mathbf{M}\mathbf{q}, \tag{13}$$

where $\mathbf{B}\mathbf{A}^{-1}\mathbf{B}^T$ is called the Schur complement.

Remark 4. In the case of an enclosed flow, the first eigenvalue is zero, since it represents the constant pressure mode. In such a case β_h is estimated by the square root of the second lowest eigenvalue. On the contrary, if the problem admits a Neumann boundary condition then all eigenvalues are strictly positive.

5. Numerical tests

In this section we propose two kinds of numerical experiments, solved both with the P_2/P_1 and P_2^+/P_1 schemes described above. We recall that, when considering the P_2^+/P_1 scheme, the bubbles are added only on the subtriangles. On all other elements the P_2/P_1 scheme is used.

The first experiment is a test in which the "inflow" condition is applied on the immersed boundary. We then study the solution of the problem on very simple meshes as the position of the immersed boundary varies. We consider three cases for the SGE-test: a constant flow, a Poiseuille flow, and a colliding flow. Each SGE-test has an analytical solution, which is presented in subsequent sections.

The second set of experiments explores three applications. The first problem is a Stokes flow around a disk, with the disk boundary being the immersed boundary. The second problem is a flow against an "obstacle" that defines a part of the boundary of the fluid domain. The third problem is a "surface" flow problem, where the surface is described by an immersed boundary.

We also provide and discuss for some representative tests the condition number, denoted by κ, of Schur complement, see Eq. (13).

Remark 5. We point out that in all presented tests integration was performed exactly. However, further numerical experiments showed that the use for P_2^+/P_1 of the integration rule exact on P_2/P_1 (clearly leading to an under-integration of the terms involving bubble shape functions) leads to practically identical results. This is in agreement with what is expected from a theoretical point of view. It thus follows that P_2^+/P_1 at a cost similar to P_2/P_1.

5.1. Smallest Generalized Eigenvalue test problems

The Smallest Generalized Eigenvalue test (SGE-test) is presented in Fig. 7. The background mesh is defined on $[-1, 1] \times [-1, 1]$ and the mesh used for the SGE-test is shown in Fig. 8. The problem consists in varying the position of an "immersed" boundary (depicted in red in Fig. 7) from -1 to 0, representing two tests:

- Test 1: $a \to 0$ with inflow positions described in Table 1(a) (examples are given in Fig. 8(a)),
- Test 2: $b \to 0$ with inflow positions described in Table 1(b) (examples are given in Fig. 8(b)).

The physical domain of the problem is on the right of the immersed boundary. We necessarily impose a Dirichlet boundary condition on the immersed boundary, which are different for each cases: the constant flow, the Poiseuille flow, and the colliding flow.

We note that in both tests the element ratio σ scales linearly. In the following, we report the numerical results relative to the different flow conditions considered.

For the first two SGE-test cases, we evaluate the results in terms of the discrete L^2-norm for both the velocity and the pressure fields. More precisely given $\hat{\mathbf{u}}_i^I = \mathbf{u}(\boldsymbol{x}_i)$ and $\hat{p}_i^I = p(\boldsymbol{x}_i)$ the analytical solution of the velocity and the pressure, respectively, at the node $\boldsymbol{x}_i$, the discrete L^2 velocity error is defined by

$$e_v = \sqrt{(\hat{\mathbf{u}}^I - \hat{\mathbf{u}})^T(\hat{\mathbf{u}}^I - \hat{\mathbf{u}})} = \|\hat{\mathbf{u}}^I - \hat{\mathbf{u}}\|_0,$$

and the discrete L^2 pressure error is defined by

$$e_p = \sqrt{(\hat{\mathbf{p}}^I - \hat{\mathbf{p}})^T(\hat{\mathbf{p}}^I - \hat{\mathbf{p}})} = \|\hat{\mathbf{p}}^I - \hat{\mathbf{p}}\|_0.$$

Please cite this article in press as: F. Auricchio, et al., An "immersed" finite element method based on a locally anisotropic remeshing for the incompressible Stokes problem, Comput. Methods Appl. Mech. Engrg. (2015), http://dx.doi.org/10.1016/j.cma.2014.10.001

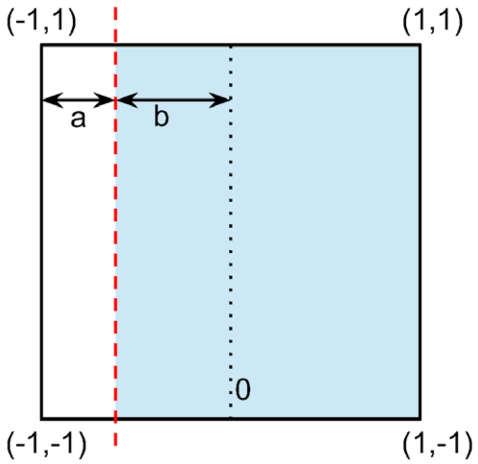

Fig. 7. Immersed boundary (dotted red), physical domain (in blue) geometric data for an SGE-test problem. (For interpretation of the references to color in this figure legend, the reader is referred to the web version of this article.)

Table 1
Geometric considerations for both tests. The highest element ratio is denoted by σ.

(a) Test 1: $a \to 0$.					
a	1e−1	1e−2	1e−3	1e−4	1e−5
σ	9.6	99.6	1.0e3	1.0e4	1.0e5
(b) Test 2: $b \to 0$.					
b	1e−1	1e−2	1e−3	1e−4	1e−5
σ	13.1	140	1.4e3	1.4e4	1.4e5

5.1.1. *Constant flow*

The first case consists in imposing a constant inflow. The boundary conditions are $u_x = 1$ and $u_y = 0$ on $x = a - 1$ for Test 1 and on $x = -b$ for Test 2, respectively. On $x = 1$ *and* $y \pm 1$ we apply the so-called "do-nothing" boundary condition, that is $\nabla \mathbf{u} \cdot \mathbf{n} - p\mathbf{n} = \mathbf{0}$, where $\mathbf{n}$ is the outward normal.

The analytical solution for the constant flow problem is given by

$$\begin{cases} u_x(x, y) = 1, \\ u_y(x, y) = 0, \\ p(x, y) = 0. \end{cases}$$

For Tests 1 and 2, (see results in Tables 2 and 3, respectively) it is clear that both elements are stable as the numerical inf–sup constant remains bounded from below. Moreover, as already pointed out, the element ratio increases linearly for both tests and thus the condition that the element ratio remains bounded from above is not a necessary condition for both finite element schemes.

The condition number of the Schur complement (see Eq. (13)) is denoted by κ. We can observe in Table 2 that for Test 1 κ scales as a^{-1}, while we see from Table 3 that for Test 2 it scales as b^{-2}. We point out that for Test 1 the smallest area of the triangles scales as a while for Test 2 it scales as b^2, leading to the different conditioning rates of the Schur complement between Test 1 and Test 2. Bounds for the conditioning of the Schur complement are provided, e.g., in [13] or in Proposition 4.47 from [27] as function of the inf–sup constant and the condition number of the pressure mass matrix. A bound for the mass matrix with anisotropic elements is provided, e.g., in [28]. The results are consistent with the theory.

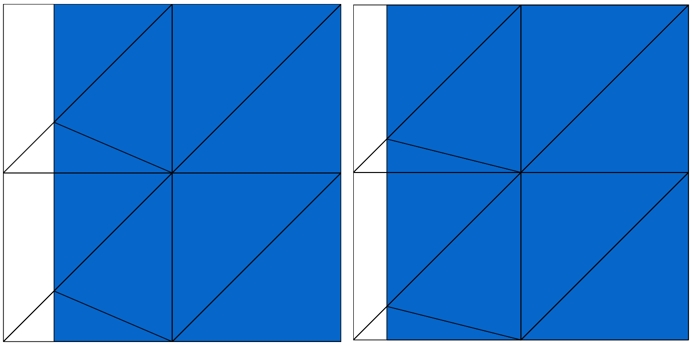

(a) Test 1: Deformation of the refined elements as a tends to 0.

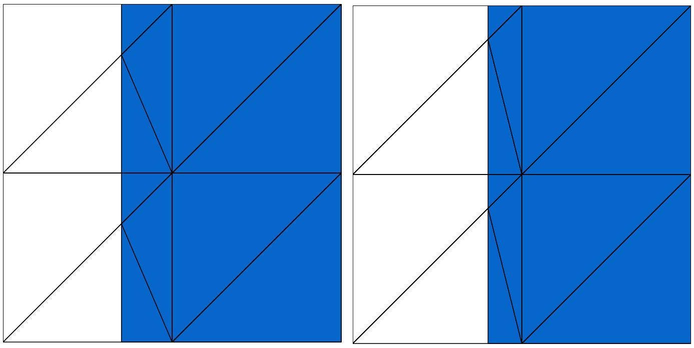

(b) Test 2: Deformation of the refined elements as b tends to 0.

Fig. 8. Mesh under consideration for the SGE-tests with different immersed boundary positions. The background domain is defined on $[-1, 1] \times [-1, 1]$. Smallest element ratios for the considered values in the two tests are depicted in Table 1.

Table 2
Constant flow Test 1: $a \to 0$.

(a) P_2/P_1					
a	1e−1	1e−2	1e−3	1e−4	1e−5
β_h	0.505	0.500	0.500	0.500	0.500
κ	4.93e+02	5.01e+03	5.07e+04	5.02e+05	5.02e+06
e_v	7.17e−15	1.41e−14	4.99e−13	1.11e−12	1.48e−12
e_p	1.50e−14	8.42e−14	3.43e−12	7.71e−12	1.15e−11
(b) P_2^+/P_1					
a	1e−1	1e−2	1e−3	1e−4	1e−5
β_h	0.667	0.636	0.633	0.632	0.632
κ	2.91e+02	3.11e+03	3.14e+04	3.14e+05	3.14e+06
e_v	1.01e−14	8.38e−15	1.11e−13	3.27e−12	3.55e−11
e_p	2.34e−14	2.76e−14	7.66e−13	2.00e−11	2.30e−10

5.1.2. *Poiseuille flow*

The second case consists in a viscous flow between two infinite plates positioned respectively on $y \pm 1$. The boundary conditions are $u_x = (1 - y^2)$ and $u_y = 0$ on $x = a - 1$ for Test 1 and $x = -b$ for Test 2. On $y = \pm 1$ the so-called "no-slip" boundary condition is applied, that is $\mathbf{u} = \mathbf{0}$. On $x = 1$ the do-nothing boundary condition is

Table 3
Constant flow Test 2: $b \to 0$.

(a) P_2/P_1

b	1e−1	1e−2	1e−3	1e−4	1e−5
β_h	0.548	0.509	0.501	0.500	0.500
κ	2.26e+03	2.65e+05	2.76e+07	2.76e+09	2.76e+11
e_v	1.79e−15	1.68e−15	1.55e−15	2.09e−15	1.73e−15
e_p	7.77e−14	2.36e−13	2.99e−12	8.47e−11	3.87e−10

(b) P_2^+/P_1

b	1e−1	1e−2	1e−3	1e−4	1e−5
β_h	0.686	0.657	0.640	0.638	0.638
κ	1.23e+03	1.42e+05	1.46e+07	1.46e+09	1.47e+11
e_v	2.09e−15	2.49e−15	1.82e−15	2.72e−15	3.17e−15
e_p	2.44e−14	7.71e−13	5.76e−12	9.46e−11	1.35e−09

Table 4
Poiseuille flow Test 1: $a \to 0$.

(a) P_2/P_1

a	1e−1	1e−2	1e−3	1e−4	1e−5
β_h	0.360	0.354	0.354	0.354	0.354
κ	2.24e+02	1.70e+03	1.65e+04	1.64e+05	1.64e+06
e_v	6.64e−16	2.66e−15	1.03e−13	2.20e−13	4.79e−12
e_v	8.09e−15	3.49e−14	1.63e−12	3.46e−12	7.56e−11

(b) P_2^+/P_1

a	1e−1	1e−2	1e−3	1e−4	1e−5
β_h	0.405	0.393	0.392	0.392	0.392
κ	1.28e+02	1.06e+03	1.03e+04	1.03e+05	1.03e+06
e_v	1.12e−15	4.46e−15	2.77e−14	1.77e−12	6.08e−12
e_v	1.69e−14	4.29e−14	2.23e−13	1.46e−11	5.03e−11

applied. The analytical solution for the Poiseuille flow problem is given by

$$\begin{cases} u_x(x,y) = (1-y^2), \\ u_y(x,y) = 0, \\ p(x,y) = 2-2x. \end{cases} \tag{14}$$

As for the constant flow, also in this case, both finite element schemes are stable for Test 1 (see Table 4).

However, for Test 2, the P_2/P_1 finite element is not stable anymore (see Table 5(a)), as the inf–sup constant decreases sublinearly (with a rate of $\mathcal{O}(b^{1/2})$) as b tends to 0. We remark that in case one uses a geometric tolerance as employed in [8] or with the XFEM, this result points out the direct dependence of the inf–sup constant on such a geometrical tolerance. The P_2^+/P_1 scheme is instead stable. The main difference with the constant flow SGE-test is the presence of Dirichlet boundary conditions on $y = \pm 1$. Further tests showed that the instability appears from the upper left corner of the domain, where a small triangle, while well shaped, has an area that decreases as $\mathcal{O}(b^2)$. We point out that, to the best of the authors' knowledge, a proof of stability of P_2^+/P_1 for anisotropic meshes has not been published.

We note that the solution for the constant flow and the Poiseuille flow is contained in the finite element spaces. Therefore, even if the numerical inf–sup constant tends to zero, the solution remains close to zero (see error estimates in Section 4).

Regarding the conditioning of the Schur complement we can observe in Table 5(a), i.e., in the case P_2/P_1 is inf–sup unstable, that the condition number worsens since it does not scale as b^{-2} but as b^{-3}. This result is consistent with the theory.

Please cite this article in press as: F. Auricchio, et al., An "immersed" finite element method based on a locally anisotropic remeshing for the incompressible Stokes problem, Comput. Methods Appl. Mech. Engrg. (2015), http://dx.doi.org/10.1016/j.cma.2014.10.001

Table 5
Poiseuille flow Test 2: $b \to 0$.

(a) P_2/P_1

b	1e−1	1e−2	1e−3	1e−4	1e−5
β_h	0.198	0.066	0.021	0.007	0.002
κ	8.51e+03	7.40e+06	7.27e+09	7.26e+12	7.26e+15
e_v	1.17e−15	8.58e−16	8.49e−16	8.64e−16	6.59e−16
e_v	1.46e−13	9.11e−13	4.39e−10	2.12e−08	2.61e−06

(b) P_2^+/P_1

b	1e−1	1e−2	1e−3	1e−4	1e−5
β_h	0.435	0.380	0.370	0.369	0.368
κ	1.43e+03	2.00e+05	2.13e+07	2.15e+09	2.15e+11
e_v	9.71e−16	9.51e−16	1.01e−15	1.35e−15	7.23e−16
e_v	1.64e−14	2.80e−13	4.89e−12	6.00e−11	3.99e−10

Table 6
Colliding flow Test 1: $a \to 0$.

(a) P_2/P_1

a	1e−1	1e−2	1e−3	1e−4	1e−5
β_h	0.369	0.367	0.366	0.366	0.367
re_v	3.90e−02	3.86e−02	3.86e−02	3.86e−02	3.86e−02
re_p	7.82e−01	7.74e−01	7.75e−01	7.75e−01	7.75e−01

(b) P_2^+/P_1

a	1e−1	1e−2	1e−3	1e−4	1e−5
β_h	0.376	0.376	0.376	0.376	0.376
re_v	4.05e−02	3.84e−02	3.83e−02	3.82e−02	3.82e−02
re_p	7.58e−01	7.77e−01	7.80e−01	7.81e−01	7.81e−01

5.1.3. Colliding flow

The third case is a colliding flow problem. In this case, we impose Dirichlet boundary condition everywhere, including the immersed boundary. They are given by the following, which is the analytical solution of the problem.

$$\begin{cases} u_x(x, y) = 20xy^3, \\ u_y(x, y) = 5x^4 - 5y^4, \\ p(x, y) = 60x^2y - 20y^3 + \text{constant}. \end{cases}$$

Since it is an enclosed flow problem, the following constraint on the pressure is added:

$$\int_\Omega p \,\mathrm{d}\Omega = 0.$$

For SGE-test case 3, we use the relative error norm, that is

$$e_{v,r} = \|\hat{\mathbf{u}}^I - \hat{\mathbf{u}}\|_0 / \|\hat{\mathbf{u}}^I\|_0,$$

and

$$e_{p,r} = \|\hat{\mathbf{p}}^I - \hat{\mathbf{p}}\|_0 / \|\hat{\mathbf{p}}^I\|_0,$$

for the velocity and the pressure, respectively.

Again for Test 1 (see Table 6) both finite element schemes are stable and for Test 2 (see Table 7) the P_2/P_1 scheme is not stable, on the contrary to the P_2^+/P_1 scheme. In this case, the analytical solution is not contained anymore in the finite element space and we can observe that, as the numerical inf–sup constant β_h tends to 0 as $b \to 0$ with a rate

Table 7
Colliding flow Test 2: $b \to 0$.

(a) P_2/P_1

b	1e−1	1e−2	1e−3	1e−4	1e−5
β_h	0.197	0.066	0.021	0.007	0.002
re_v	5.23e−02	6.23e−02	6.56e−02	6.60e−02	6.60e−02
re_p	3.66e+00	5.03e+01	5.33e+02	5.37e+03	5.37e+04

(b) P_2^+/P_1

b	1e−1	1e−2	1e−3	1e−4	1e−5
β_h	0.360	0.335	0.328	0.327	0.327
re_v	5.22e−02	6.22e−02	6.56e−02	6.60e−02	6.60e−02
re_p	1.14	2.17	2.45	2.48	2.49

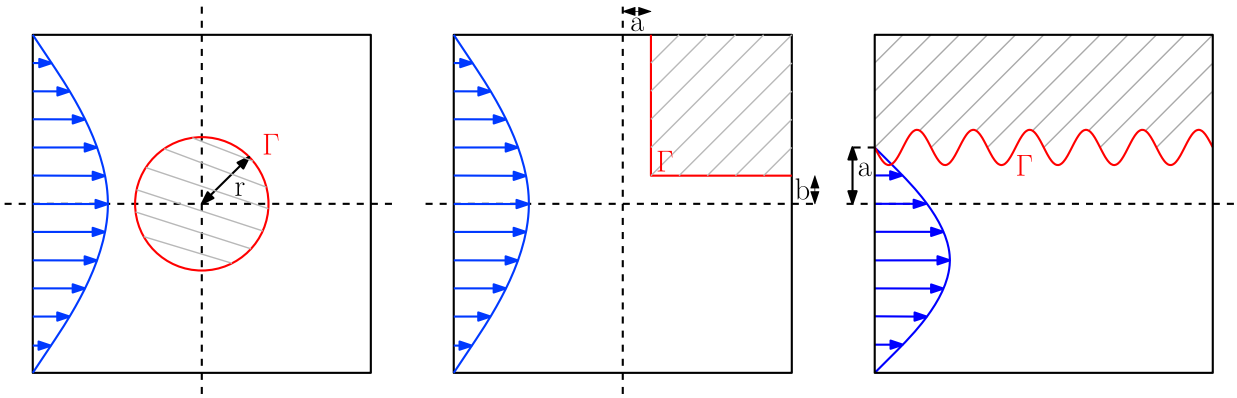

(a) Flow around a disk. (b) Flow against an obstacle. (c) Surface flow.

Fig. 9. Three flow problems. The striped zone is excluded from the fluid domain.

of $\mathcal{O}(b^{1/2})$, the relative pressure error explodes linearly, which is in accordance with the error estimates in Eq. (10). On the contrary, the velocity error remains bounded, which is not expected from the error estimate in Eq. (9). More precisely, we would expect the velocity error to increase with an order of $\mathcal{O}(b^{1/2})$. However, a good velocity field with a bad pressure field is often seen, for example with the Q_1/P_0 scheme.

5.2. Applications

In this section, we present various possible applications as described in Fig. 9. For the first experiment (see Fig. 9(a)), we compare a fitted and an unfitted solution. We also investigate some extreme cases, with very anisotropic elements that can occur during simulations. We show that the P_2/P_1 is actually stable for that problem. Nevertheless, we show that the solution using the P_2^+/P_1 is smoother. Then, we present two additional applications (described in Fig. 9(b) and (c)) for which the P_2/P_1 fails, while P_2^+/P_1 is stable. For both failing cases, the culprit is a very small triangle in corners for which Dirichlet boundary conditions are applied on both boundary edges, as found in the SGE-tests. For all tests we do not present the results for the velocity field but the solution is in accordance with those obtained with the SGE-tests, i.e., the accuracy of the velocity field remains very good even when highly anisotropic elements are present.

5.2.1. Flow around a disk

We here consider a problem consisting of a flow around a cylinder between two plates. By symmetry, the problem reduces to a 2D flow around a disk, whose boundary is defined as an immersed boundary (see Fig. 9(a)). The fluid domain is defined on $[-1, 1] \times [-1, 1]$. The inflow condition is a Poiseuille inflow and is given by Equation (14), no-slip boundary conditions are prescribed on $y = \pm 1$ and a do-nothing boundary condition is applied on $x = 1$. The

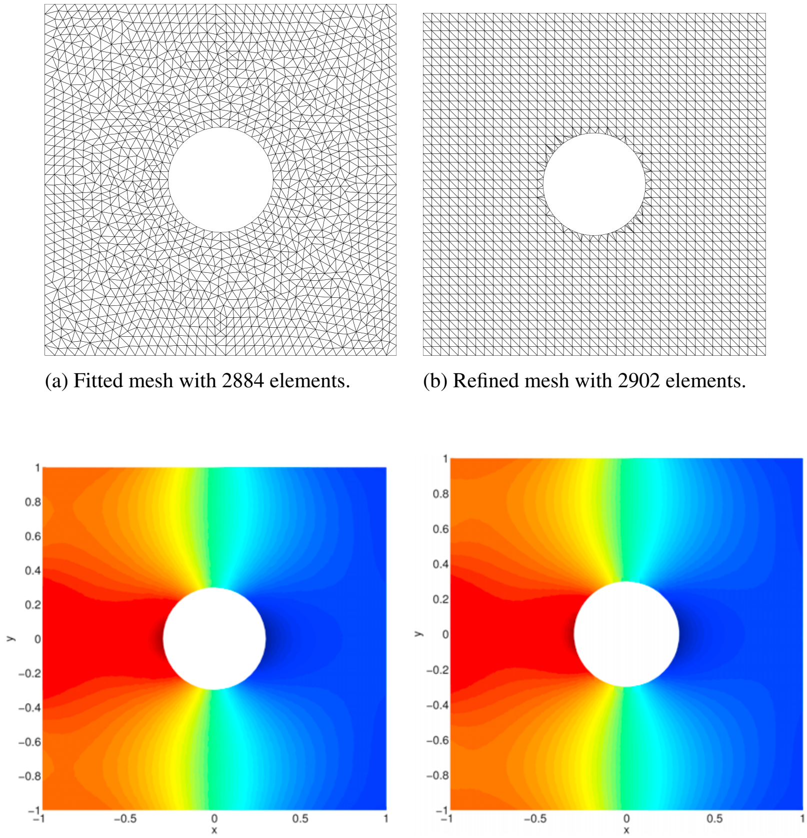

(a) Fitted mesh with 2884 elements. (b) Refined mesh with 2902 elements.

(c) Fitted mesh pressure. (d) Refined mesh pressure.

Fig. 10. Solution of the incompressible Stokes problem around a disk with the P_2/P_1 and a Poiseuille inflow. The radius of the disk is 0.3.

disk has a radius of 0.3 and a no-slip boundary condition is applied on its surface. A comparison between a standard finite element solution and the proposed method is presented in Fig. 10 with the P_2/P_1 scheme for both methods. We can observe that the solution is similar to a standard finite element solution, and thus the presented method provides an accurate solution of the problem.

In the following we discuss in more details possible effects of anisotropic elements with the P_2/P_1 and the P_2^+/P_1 elements. We present two cases with highly anisotropic elements. The first one with a background mesh of 11×11 quadrilaterals and the second with a background mesh of 23×23 quadrilaterals, then divided into triangles with their diagonals such that $x - y =$ constant. The results are presented in Fig. 11. We observe that the inf–sup constant is identical ($\beta_h \approx 0.18$) for both finite element schemes on meshes with anisotropic elements, and thus indicating stability of both schemes. However, we can see that the P_2^+/P_1 solution is smoother than the pressure solution with the P_2/P_1 element. Also, the oscillations appear to vanish as the mesh size is reduced. We point out that, in this problem, none of the anisotropic elements are recessed in a corner with Dirichlet boundary conditions applied on both corner sides. This situation occurs in the constant SGE-test problem for which both finite element schemes are stable for all tests. Therefore, it is possible that for many practical applications the P_2/P_1 element is actually stable.

5.2.2. *Flow against an obstacle*

In this problem (depicted in Fig. 9(b)) we consider a flow problem against an "obstacle". In this particular case the immersed boundary is not closed and defines a part of the outer boundary of the fluid domain. The background fluid domain is defined on a $[-1, 1] \times [-1, 1]$ discretized by a mesh of 43×43 quadrilaterals subdivided into triangles with their diagonals such that $x + y =$ constant and the immersed boundary as described on Fig. 9(b). For the present test we set $a = -0.333$ and $b = 0.3333$.

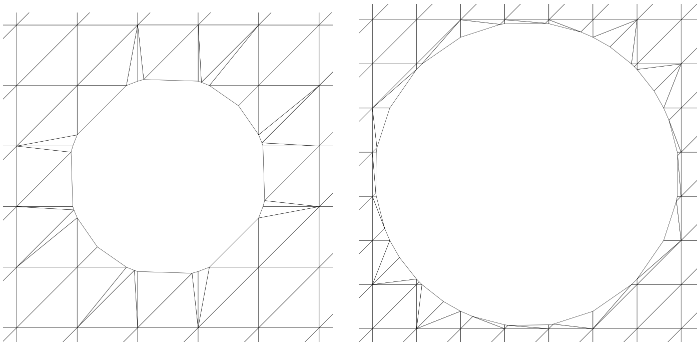

(a) Locally refined with a background mesh 11 × 11.

(b) Locally refined with a background mesh 23 × 23.

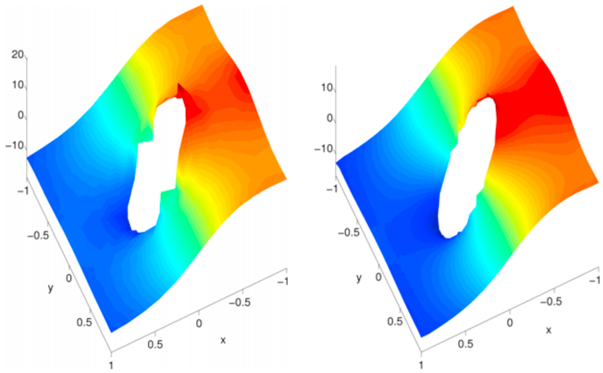

(c) Pressure field P_2/P_1; $\beta_h \approx 0.183$.

(d) Pressure field P_2/P_1; $\beta_h \approx 0.182$.

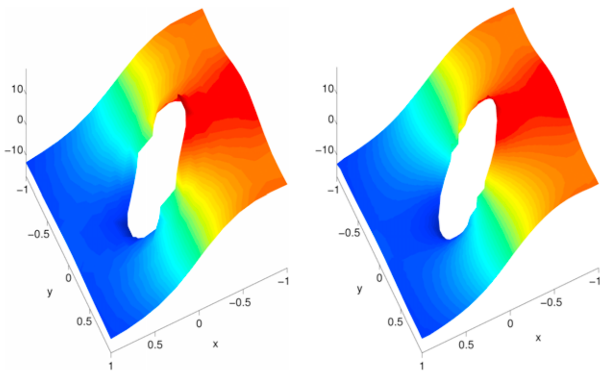

(e) Pressure field P_2^+/P_1; $\beta_h \approx 0.183$.

(f) Pressure field P_2^+/P_1; $\beta_h \approx 0.182$.

Fig. 11. Effects of anisotropic elements for two different meshes (11 × 11) and (23 × 23). The immersed boundary has a radius of 0.3 and it is discretized with 89 linear elements.

The boundary conditions are applied as follows. On $x = -1$ the Poiseuille inflow is applied (see Eq. (14)). On $y = 1$, $x = 1$, and Γ, no-slip boundary conditions are applied. On $y = -1$ we impose the do-nothing boundary condition.

Computations show (see Fig. 12) that the numerical inf–sup constant is smaller for the P_2/P_1 element with $\beta_h \approx 0.054$ than for the P_2^+/P_1 with $\beta_h \approx 0.265$. The numerical inf–sup constant for the P_2^+/P_1 is in the range of the stable cases presented in the SGE-tests (see Section 5.1), while for the P_2/P_1 scheme it is an order of magnitude

Please cite this article in press as: F. Auricchio, et al., An "immersed" finite element method based on a locally anisotropic remeshing for the incompressible Stokes problem, Comput. Methods Appl. Mech. Engrg. (2015), http://dx.doi.org/10.1016/j.cma.2014.10.001

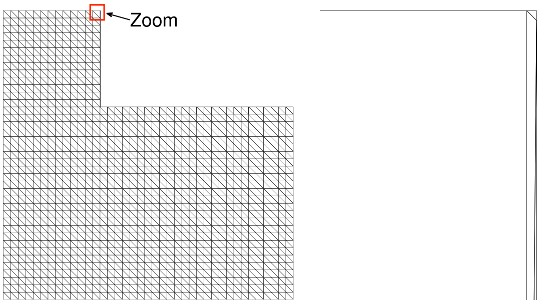

(a) Mesh of 43 × 43 on $[-1, 1] \times [-1, 1]$.

(b) Zoom.

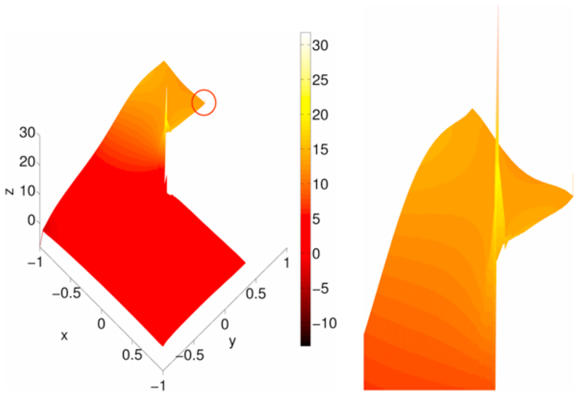

(c) Pressure solution for P_2/P_1; $\beta_h \approx 0.054$.

(d) Zoom on locking effect for the P_2/P_1 element.

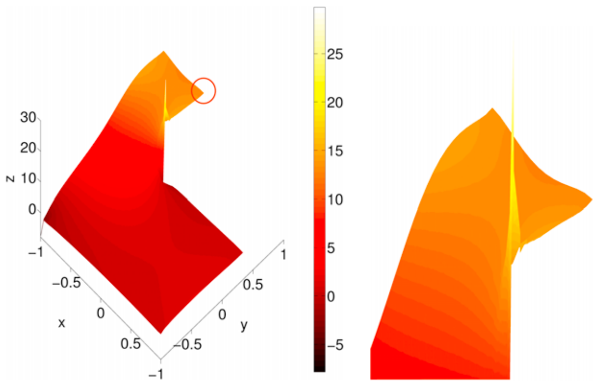

(e) Pressure solution for P_2^+/P_1; $\beta_h \approx 0.265$.

(f) Zoom where no locking effects are visible with the P_2^+/P_1 element.

Fig. 12. Presentation of the "obstacle" problem and results. In particular, locking effects are present for the P_2/P_1 element. We note that it occurs in a small triangle in the corner (see zoom 12(d)) with Dirichlet boundary condition, as in the Poiseuille SGE-test.

smaller than stable values. We can observe the effect of locking in Fig. 12(d) and absence of locking for the P_2^+/P_1 element in Fig. 12(f). The culprit is due to a small triangle recessed in the upper right corner (see Fig. 12(a) and (b)). The locking effect is observed only on a triangle in a small corner with Dirichlet boundary conditions on both edges, thus reflecting the results obtained in the Poiseuille and colliding SGE-tests. In that situation the P_2/P_1 element is unstable for the Poiseuille and colliding Test 2. However, the locking effects are quite small as it can be seen by

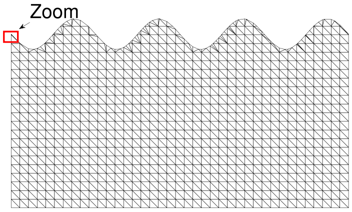

(a) Background mesh with subdivided elements defined by Γ.

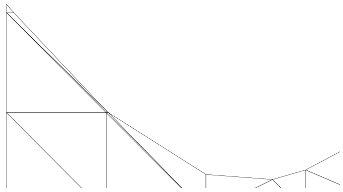

(b) Zoom: a small triangle in the corner with Dirichlet boundary as in the Poiseuille SGE-test.

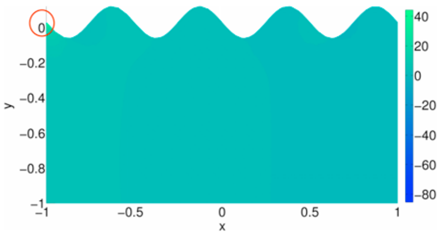

(c) Pressure solution for P_2/P_1; $\beta_h \approx 0.064$.

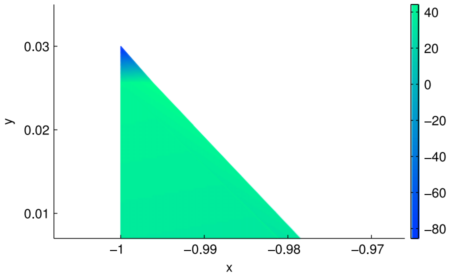

(d) Zoom on locking effect for the P_2/P_1 element.

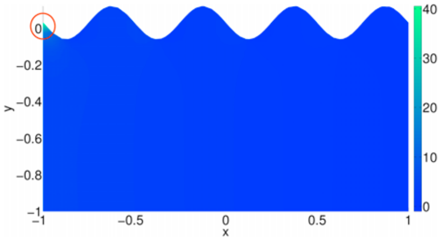

(e) Pressure solution for P_2^+/P_1; $\beta_h \approx 0.208$.

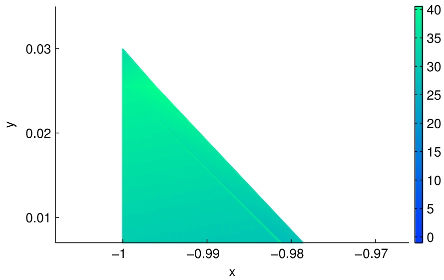

(f) Zoom where no locking effects are visible with the P_2^+/P_1 element.

Fig. 13. Presentation of the mesh and results for the "free surface" flow problem. Locking effects are visible (wrong value (−80) of the pressure on the upper left corner triangle) for the P_2/P_1 scheme and absent for the P_2^+/P_1 scheme.

comparing Fig. 12(c) with Fig. 12(e). We point out that the peak of pressure for both elements is due to the irregularity of the solution resulting from the L-shaped immersed boundary.

5.2.3. A "surface" flow problem

In this problem (represented in Fig. 9(c)) we consider a "surface" flow, where the surface is described as an immersed boundary. The background mesh is defined on a $[-1, 1] \times [-1, 1]$ discretized by a mesh of 43×43 quadrilaterals subdivided in triangles with their diagonals such that $x + y =$ constant. The surface Γ is represented by $y = 0.03 - (1/11)\sin(4\pi x)$ and it is discretized by 1001 segments. On $x = -1$ and $y = [-1, 0.03]$ we impose $\mathbf{u} = \{(0.03 - x)(1 + x), 0\}^T$. On $y = -1$ and Γ a no-slip boundary condition and on $x = 1$ and $y = [-1, 0.03]$ a do-nothing boundary conditions are applied.

For this problem similar results as with the obstacle problem are obtained, that is, a much lower numerical inf–sup constant ($\beta_h \approx 0.064$) is obtained for the P_2/P_1 element than for the P_2^+/P_1 element ($\beta_h \approx 0.208$). The inf–sup values suggest a possible locking effect with the P_2/P_1 element. Indeed, looking at Fig. 13(c) a very low pressure value is present (around −80), while such a low pressure is absent in the pressure field with the P_2^+/P_1 element (see Fig. 13(e)). Looking at the zooms (Fig. 13(d) and (f)), we can observe that the very low pressure value for the P_2/P_1

element arises on the upper (small) triangle (see Fig. 13(b)), for which, on two of its edges we impose a Dirichlet boundary condition. On the contrary, for the P_2^+/P_1 we obtain a satisfactory value.

6. Conclusions

In this paper we presented an immersed grid method, in which the immersed boundary was reconstructed linearly (but the linear reconstruction of the interface is not a restriction of the method). The reconstruction was performed locally (i.e., at the element level) which requires the computation of intersection points with the background mesh. The previously described steps are common to most *eXtended Finite Element Method* (XFEM) implementations. The presented method differs from XFEM since each element intersected by the immersed boundary were subdivided into subelements on which we reconstructed a finite element basis, as in a refined approach. Advantages are twofold. Firstly, we obtain an accurate representation of the immersed boundary. Secondly, it is very easy to impose Dirichlet boundary condition on the immersed boundary. However, the subdivision may induce highly anisotropic elements. In this paper, we focused on the case of the P_2/P_1 element and pointed out its defects; in particular, we show that for our application the P_2/P_1 scheme may not be inf–sup stable when elements are highly anisotropic. Numerical investigations showed that locking effects may occur on anisotropic elements in corners for which Dirichlet boundary conditions are imposed on both edges. Therefore, the stability of the element may be guaranteed for a large class of problems, but not for all as showed. Nevertheless, we presented a solution which consists in enriching the velocity space with a bubble (named herein P_2^+/P_1). It was shown numerically that such a finite element scheme is inf–sup stable in all presented tests.

Two relevant issues have not been addressed by this work, i.e., the influence of the conditioning of the various matrices with anisotropic elements and the extension of the refinement strategy to 3D. Both problems will be the subject of future works. In particular, the conditioning issue may have an important impact in situations such as transient problems (see, e.g., Remark 4.48(ii) in [27]). About the extension to 3D, we have to note that the subdivision of tetrahedra leads to sliver tetrahedra and results on 2D anisotropic meshes cannot be, in general, straightforwardly extended to 3D. For instance, in [29] it is discussed an analogue of the maximal angle condition for triangles to linear tetrahedra. Inf–sup stability in such cases remains a difficult problem. Nevertheless, our envisioned solution is to use a recently developed numerical method named the Virtual Element Method (VEM) (see, e.g., [30,31]). This approach has two important properties that could be employed in the framework discussed in this article: it allows elements to be arbitrary polytopes (and thus we can avoid the subdivision process) and it is robust when elements are highly anisotropic.

Acknowledgments

This work is funded by: the Cariplo Foundation through the Project no. 2009.2822; the European Research Council through the ERC Starting Grant Project no. 259229; Ministero dell'Istruzione, dell'Università e della Ricerca through the PRIN Project no. 2010BFXRHS.

References

[1] J. Haslinger, Y. Renard, A new fictitious domain approach inspired by the extended finite element method, SIAM J. Numer. Anal. 47 (2009) 1474–1499.
[2] T.-P. Fries, T. Belytschko, The extended/generalized finite element method: An overview of the method and its applications, Int. J. Numer. Meth. Engng. 84 (2010) 253–304.
[3] J. Sanders, T. Laursen, M. Puso, A Nitsche embedded mesh method, Comput. Mech. 49 (2012) 243–257.
[4] F. Ilinca, J.-F. Hétu, A finite element immersed boundary method for fluid flow around rigid objects, Internat. J. Numer. Methods Fluids 65 (2011) 856–875.
[5] R. Löhner, Applied Computational Fluid Dynamics Techniques, An Introduction Based on Finite Element Methods, John Wiley and Sons, 2008.
[6] P. Frey, P.-L. George, Mesh Generation, Wiley, 2008.
[7] R. van Loon, P. Anderson, J. de Hart, F. Baaijens, A combined fictitious domain/adaptive meshing method for fluid–structure interaction in heart valves, Int. J. Numer. Meth. Fluids 46 (2004) 533–544.
[8] R. van Loon, P. Anderson, F. van de Vosse, A fluid–structure interaction method with solid-rigid contact for heart valve dynamics, J. Comput. Phys. 217 (2006) 806–823.
[9] T. Apel, H. Randrianarivony, Stability of discretizations of the Stokes problem on anisotropic meshes, J. Math. Comput. Simul. 61 (2003) 437–447.

[10] A. Hansbo, P. Hansbo, An unfitted finite element method, based on Nitsche's method, for elliptic interface problems, Comput. Methods Appl. Mech. Engrg. 191 (2002) 5537–5552.

[11] J. Parvizian, A. Düster, E. Rank, Finite cell method, Comput. Mech. 41 (2007) 121–133.

[12] S. Basting, M. Weismann, A hybrid level set-front tracking finite element approach for fluid–structure interaction and two-phase flow applications, J. Comput. Phys. 255 (2013) 228–244.

[13] D. Boffi, F. Brezzi, M. Fortin, Mixed Finite Element Methods, Springer, 2013.

[14] A. Lew, G. Buscaglia, A discontinuous-Galerkin-based immersed boundary method, Int. J. Numer. Meth. Engng. 76 (2008) 427–454.

[15] B. Maury, Numerical analysis of a finite element/volume penalty method, SIAM J. Numer. Anal. 47 (2) (2009) 1126–1148.

[16] E. Béchet, N. Moës, B. Wohlmuth, A stable Lagrange multiplier space for stiff interface conditions within the extended finite element method, Int. J. Numer. Meth. Engng. 78 (2009) 931–954.

[17] E. Burman, P. Hansbo, Fictitious domain methods using cut elements: III. A stabilized nitsche method for Stokes' problem, Tech. Rep., Jönköping University, 2011.

[18] J. Baiges, R. Codina, F. Henke, S. Shahmiri, W. Wall, A symmetric method for weakly imposing dirichlet boundary conditions in embedded finite element meshes, Int. J. Numer. Meth. Engng (2012).

[19] S. Court, M. Fournier, A. Lozinski, A fictitious domain approach for the stokes problem based on the extended finite element method, Int. J. Numer. Meth. Fluids 74 (2014) 73–99.

[20] M. Zlámal, On the finite element method, Numer. Math. 12 (1968) 394–409.

[21] A. Ženíšek, The convergence of the finite element method for boundary value problems of a system of elliptic equations, Apl. Mat. 14 (1969) 355–377. (in czech).

[22] I. Babuška, A. Aziz, On the angle condition in the finite element method, SIAM J. Numer. Anal. 13 (2) (1976) 214–226.

[23] P. Jamet, Estimations d'erreur pour des éléments finis droits presque dégénérés, RAIRO Anal. Numér. 10 (1976) 43–60.

[24] A. Hannukainen, S. Korotov, M. Křížek, The maximum angle condition is not necessary for convergence of the finite element method, Numer. Math. 120 (2012) 79–88.

[25] F. Auricchio, F. Brezzi, C. Lovadina, Mixed finite element methods, in: Encyclopedia of Computational Mechanics, John Wiley & Sons, 2004, (Chapter 9).

[26] D. Elman, H. Silvester, A. Wathen, Finite Elements and Fast Iterative Solvers with Applications in Incompressible Fluid Dynamics, Oxford Press, 2005.

[27] A. Ern, J.-L. Guermond, Theory and Practice of Finite Elements, Springer, 2004.

[28] L. Kamenski, W. Huang, H. Xu, Conditioning of finite element equations with arbitrary anistropic meshes, Math. Comput. 83 (289) (2014) 2187–2211.

[29] M. Křížek, On the maximum angle condition for linear tetrahedral elements, SIAM J. Numer. Anal. 29 (2) (1992) 513–520.

[30] L.B. da Veiga, F. Brezzi, A. Cangiani, G. Manzini, L. Marini, A. Russo, Basic principles of virtual element methods, Math. Models Methods Appl. Sci. 23 (2013) 199–214.

[31] L.B.o. da Veiga, F. Brezzi, L. Marini, A. Russo, The hitchhiker's guide to the virtual element method, Math. Models Methods Appl. Sci. 24 (2014) 1541–1573.

Please cite this article in press as: F. Auricchio, et al., An "immersed" finite element method based on a locally anisotropic remeshing for the incompressible Stokes problem, Comput. Methods Appl. Mech. Engrg. (2015), http://dx.doi.org/10.1016/j.cma.2014.10.001